Atomistic modeling of hydrocarbon systems using analytic bond-order potentials

M. Mrovec [a,b], M. Moseler [a,c], C. Elsässer [a,b], P. Gumbsch [a,b]

[a] *Fraunhofer-Institute for Mechanics of Materials IWM, Wöhlerstr. 11, 79108 Freiburg, Germany*

[b] *University of Karlsruhe, IZBS, Kaiserstr. 12, 76131 Karlsruhe, Germany*

[c] *Freiburg Materials Research Center, Stefan-Meier-Str. 21, 79104 Freiburg, Germany*

Abstract

The latest development of Pettifor's bond-order approach – the analytic bond-order potentials (ABOPs) – represents a significant improvement over the empirical potentials of the Abell-Tersoff-Brenner type. This article aims at a critical evaluation of this promising novel scheme for the hydrocarbon system and assesses its applicability to realistic large-scale atomistic simulations. It is shown that ABOP reproduces the underlying orthogonal tight-binding model accurately for both hydrocarbon molecules and carbon crystalline phases in their ground-state configurations. However, in order to reproduce also non-equilibrium configurations it is necessary to extend the σ bond order expression to account for the non-negligible sp atomic energy level separation of carbon. While the Brenner hydrocarbon potential exhibits several deficiencies in the description of amorphous hydrocarbon films, the extended ABOP model comes closer to results of accurate nonorthogonal tight-binding calculations. Remaining discrepancies of ABOP can be traced back to the limitations of the underlying orthogonal tight-binding model and its parameterization.

Key words: bond-order potentials, atomistic modeling, molecular dynamics, tight-binding models, empirical potentials
PACS: 61, 71.15Nc, 71.15Pd

Email address: matous.mrovec@iwm.fraunhofer.de (M. Mrovec).

1 Introduction

Carbon, after H, He and O the most abundant element of the universe, exhibits an outstanding flexibility in its bonding behavior. The ability to form sp, sp^2 and sp^3 hybridized electronic states gives rise to a variety of different phases which often show extraordinary properties. The hardness of diamond and fullerene-derived materials [1], the superlubricity of graphite [2], the stability of fullerenes [3], the tensile strength of carbon nanotubes [4], or the ultrasmoothness of diamond-like carbon films [5] are representative examples of extreme material properties. Consequently, there is a strong scientific and technological interest in the understanding of existing carbon and hydrocarbon based materials as well as in the prediction of novel phases and nanoscale structural composites.

In general, material properties originate from the interplay of valence electrons and ionic cores, and therefore a faithful theoretical description requires a quantum-mechanical treatment of the electronic system as well as a classical atomistic treatment of the atomic nuclei. Present computational resources in combination with an efficient mean-field treatment of the electronic many-body problem (for instance using first-principles density functional theory [6,7] or semi-empirical tight-binding methods [8–10]) allow for the investigation of static structural and short-time dynamical properties of C systems consisting of up to several thousand atoms. However, large unit cells, extended nanostructures and long-time dynamical processes are still out of reach of these powerful computational tools.

Traditionally, larger carbon systems have been treated with empirical interatomic potentials avoiding the order(N^3) bottleneck (N: number of electrons) of the electronic-structure methods caused by the exact diagonalization of the Schrödinger equation. In his pioneering work, Abell [11] introduced bond order concepts into the description of interatomic forces. Tersoff [12] applied and extended Abell's formalism to the semi-empirical atomistic treatment of pure carbon phases. Brenner [13] continued along this line by generalizing Tersoff's ansatz to develop the interatomic potential for the hydrocarbon system. Although Abell-Tersoff-Brenner type potentials have been frequently and successfully used in large-scale molecular dynamics simulations of C and C–H systems, predictions of these methods should be interpreted with caution. The mixture of theoretically justified concepts with *ad hoc* ansatz functions combined with ambiguous fits to experimental quantities often results in a limited transferability. Needless to say, that the aforementioned bonding flexibility of carbon aggravates this problem even further.

Presumably it was the unease with the nonphysical functional forms and cumbersome parameter fitting, which inspired David Pettifor and his coworkers

to break with the tradition of empirical concepts, and to develop the theory of bond-order potentials (BOPs) [14] which can be applied for a rigorous derivation of classical interatomic potentials. This was demonstrated during the development of the so-called analytic bond-order potentials (ABOPs) for the sp-valent systems [15–19], which are based on a well controlled chain of approximations starting from a given quantum-mechanical tight-binding Hamiltonian. In spite of the fact that the ABOP for the C–H system has been developed and published several years ago [17–19], applications and critical evaluations of this promising potential are still missing in the literature. The present article intends to close this gap.

The paper is organized in the following way. First, the simulation of film growth is posed as a practical problem and as an additional motivation for the need of more accurate interatomic potentials in Section 2. Thereafter the basic ABOP theory is reviewed in Section 3. This section also presents an important extension of the σ bond order expression which accounts for the non-negligible sp atomic energy level separation of carbon. In Section 4 we evaluate the ABOP model for the hydrocarbon system and elucidate which conditions have to be fulfilled in order to obtain results that are close to those of the underlying orthogonal tight-binding model. In Section 5, first applications of ABOP to realistic large-scale molecular-dynamics studies are reported. The paper ends with a conclusion on the directions for the future development of ABOPs.

2 Multiscale simulations of diamond-like carbon film growth

Diamond-like carbon (DLC), also known as tetrahedral amorphous carbon (ta-C), is an amorphous carbon phase with a high fraction of sp^3 bonds and a density close to that of diamond [20]. DLC films have widespread applications as protective coatings, for instance on magnetic and optical storage disks, optical windows, bearings, and in biomedical as well as micro-electro-mechanical systems. The combination of diamond-like properties and extreme smoothness is the key factor for the technological importance of these films.

Recently, we succeeded to explain the extreme smoothness of ta-C coatings by an atomistic/continuum multiscale model [5]. The deposition of carbon with 100 eV kinetic energy on an initially rough ta-C film (see Fig. 1) was simulated employing the modified Brenner potential [21]. Surprisingly, the initial roughness was quenched already after the impact of 4000 atoms (Fig. 1). We showed that the observed smoothing occurred due to impact induced downhill currents in the top layer of the sloped parts of the growing film and a consequent erosion of hills into neighboring hollows. The strength of these currents was calculated using independent molecular dynamics simulations and formed

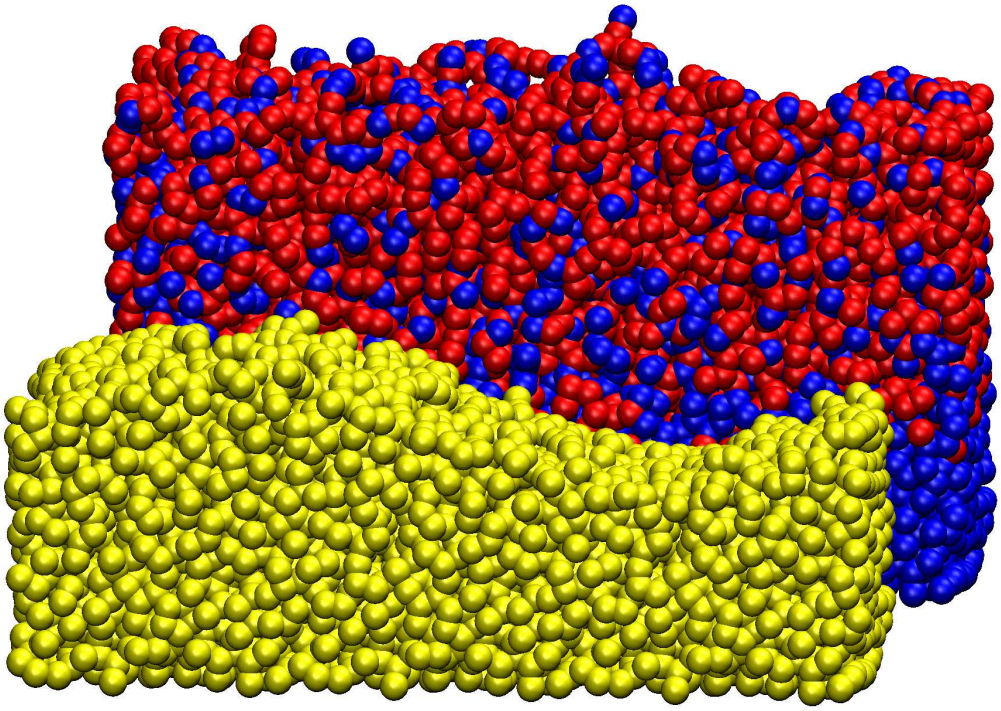

Fig. 1. Illustration of surface smoothing of a DLC film. The rough film in the foreground (yellow atoms) was bombarded by 4000 carbon atoms (red) with 100 eV impact energy. The final film (red and blue atoms in the background) shows a significant smoothing of the initial roughness.

the crucial input for a continuum-scale description of the film profile evolution. The corresponding continuum model predicted a surface evolution which was in excellent agreement with atomic force microscopy measurements from the Cambridge DLC group (see Ref. [5]).

An application of empirical potentials in complex studies, such as the growth of amorphous films, is unavoidable due to extensive lengthscales and timescales involved. At the same time the complexity and variability of the underlying processes (e.g. chemical reactions, stress relaxations, thermal treatments) places extremely high demands on the quality of interatomic potentials which have to remain accurate under equilibrium as well as non-equilibrium conditions. Simulations of ta-C films represent an important example which reveals the limited transferability of the classical potentials of Tersoff and Brenner. For this material class, both potentials fail to describe the correct fraction of sp^3 hybridized atoms and its dependence on the density [22] which are crucial material characteristics of DLC films. Jäger and Albe showed that it is possible to improve results of the Brenner potential for higher densities by simply increasing the interaction range of the potential [21]. Although this approach might be justified from a practitioner's point of view, in our opinion it is unsatisfactory and even quite uncomfortable. In our studies of film

smoothing, additional tight-binding simulations had to be performed to verify the results of the modified Brenner potential. Such higher-level calculations are very computational demanding and time consuming. Fortunately, a rough agreement between the strength of the currents of both methods was observed but even this conclusion cannot guarantee a general transferability of the modified scheme. It will become evident in the next sections that the reasonable performance of the modified Brenner potential for the ta-C films is rather fortuitous and related to the high density of the ta-C phase. When both original and modified Brenner potentials are applied to studies of hydrogenated amorphous carbon (a-C:H), both potentials show severe limitations and favor graphitic structures for the characteristic densities observed in the growth experiments. It is therefore highly desirable to have a more accurate interatomic potential for the C and C–H system which could be applied safely and without limitations in future growth studies of the technologically most important hydrogenated DLC films.

3 Theory of ABOPs

The analytic bond-order potential for the hydrocarbon system has been derived recently by Pettifor and Oleinik. The developments of the potential and basic tests are presented in three subsequent papers [17–19]. The theory of ABOPs has been extended to a general multicomponent sp-valent system in Ref. [23]. This section reviews the basic physical foundations on which the ABOPs are built, and provides the major steps which lead to analytic expressions for the bond order. For more details of the derivations the reader is refered to the paper of Drautz et al. in this volume and original papers and references therein.

3.1 The orthogonal tight-binding model

The derivation of ABOPs starts from the two-center, orthogonal tight-binding (OTB) model which can be regarded as one of the simplest models that implicitly contain the electronic structure [24]. An important advantage of the OTB model is that due to its simplicity it also provides a clear insight into the nature of bonding in terms of the chemical view of saturated and unsaturated atomic bonds. The model is thus an appropriate starting point for a rigorous derivation of interatomic potentials which are based on the intuitive concept of chemical bonds but at the same time have a sound physical root in quantum-mechanical concepts of electronic states.

The relation between the OTB model and the Kohn-Sham formulation of

the density functional theory of the electron gas [6,7] has been elaborated by Sutton et al. [25], and by Foulkes and Haydock [26]. These authors have also reformulated the classical TB *band* model into the TB *bond* model according to which the total binding energy of a non-magnetic system is given as

$$E_B = E^{rep} + E^{prom} + E^{bond}. \tag{1}$$

A more detailed discussion of this equation is given by Finnis in the introductory paper and in Ref. [27]. The first energy term accounts for the electrostatic repulsion of the ionic cores and the short-range repulsion of overlapping orbitals due to Pauli's principle. It is usually written as a sum of pairwise interactions

$$E^{rep} = \frac{1}{2}\sum_{i\neq j}\phi_{ij}. \tag{2}$$

The pairwise form of the repulsive term has no rigorous justification [27] and it is used mainly for convenience. It has been shown [8,28,29] that a more complicated form of the repulsive potential including many-body interactions can lead to a more realistic and transferable model.

The second term in Eq. (1) is also repulsive and represents the penalty of promoting a certain amount of electrons into higher-energy orbitals when atoms bond together. In the case of the hydrocarbon system, this promotion energy reflects the change of the hybridization state of the sp orbitals on carbon atoms with respect to the atomic s^2p^2 ground state, and it is given by

$$E^{prom} = \sum_i (\epsilon_p^C - \epsilon_s^C)(\Delta N_p)_i^C. \tag{3}$$

$(\epsilon_p^C - \epsilon_s^C)$ is the energy difference between atomic valence s and p energy levels of carbon which is assumed to be independent of the environment and therefore constant.

The third term in Eq. (1) is the attractive covalent bond energy which describes the cohesion of atoms. It is equal to the sum of the covalent energies of individual bonds between orbitals on different atoms

$$E^{bond} = \sum_{i\alpha\neq j\beta} \Theta_{j\beta,i\alpha} H_{i\alpha,j\beta} \tag{4}$$

where $H_{i\alpha,j\beta}$ are the Hamiltonian matrix elements and $\Theta_{j\beta,i\alpha}$ the bond order matrix elements between the orbitals $|i\alpha\rangle$ and $|j\beta\rangle$. Using the two-center representation of Slater and Koster [30], the inter-site Hamiltonian matrix elements can be expressed directly in terms of distance-dependent two-center integrals, which are known as bond or hopping integrals, and appropriate functions of directional cosines.

The bond order is defined as one half of the difference between the number of

electrons in the bonding, $\frac{1}{\sqrt{2}}\left(|i\alpha\rangle + |j\beta\rangle\right)$, and anti-bonding, $\frac{1}{\sqrt{2}}\left(|i\alpha\rangle - |j\beta\rangle\right)$, states and thus can be regarded as a measure of the strength of the bond between the orbitals $|i\alpha\rangle$ and $|j\beta\rangle$. It attains its maximum value of unity when the bonding state is totally occupied by two electrons with opposite spins and the anti-bonding state remains empty (for example, in the hydrogen dimer). In more complex molecules or in solids, however, bonds are usually unsaturated due to the influence of the surrounding atoms, and as a result, their bond orders are less than unity. It is also important to note that the bond order is not a pairwise quantity but it is dependent on the environment of atoms i and j.

Eq. (4) is the defining equation of the bond-order potential formalism. It expresses the strength of each bond in a simple way as a product of the bond order and the bond integral. In the standard TB approach the binding (i.e. band) energy, and therefore indirectly also the bond orders, are calculated by solving the Schrödinger equation in a minimal-basis-set matrix representation. The essential achievement in the ABOP development is to express the bond orders in the form of analytic functions of bond lengths and bond angles. In practice this is done by a many-body expansion of the bond order described in the following section.

3.2 The analytic bond orders

The starting equation for the evaluation of the bond order is its expression in terms of the elements of the Hamiltonian Green's function matrix [14]

$$\Theta_{i\alpha,j\beta} = -\frac{2}{\pi} \lim_{\eta \to 0} \mathrm{Im} \left\{ \int_{-\infty}^{E_F} G_{i\alpha,j\beta}\left(E + i\eta\right)\, dE \right\}. \tag{5}$$

To obtain the inter-site Green's function matrix elements in an accurate and efficient way is not a simple matter, and it requires several necessary ingredients. To describe these properly would require a separate section for each of them. We therefore refer the reader to papers by Finnis, by Aoki et al. and by Drautz et al. in this volume which give detailed discussions of this process, and we restrict ourselves to merely naming the fundamental ideas necessary for the understanding.

The first key ingredient on the way to the bond order is the recursion method [31]. The basis of the recursion method is the Lanczos algorithm [32] for tridiagonalization of sparse matrices. When applied to the Hamiltonian, this algorithm enables to write the diagonal elements of the single-particle Green's function explicitly in terms of the elements of the tridiagonalized Hamiltonian,

commonly called the recursion coefficients, as a continued fraction

$$G_{00}(E) = \cfrac{1}{E - a_0 - \cfrac{(b_1)^2}{E - a_1 - \cfrac{(b_2)^2}{E - a_2 - \cfrac{(b_3)^2}{\ddots}}}} \tag{6}$$

The recursion coefficients a_n and b_n are related to the moments of the local density of states μ_p. Another powerful identity [33,34] states that the p-th moment of the density of states projected onto the orbital $|i\alpha\rangle$ equals to the p-th moment of the Hamiltonian projected onto the same orbital

$$\mu_{i\alpha}^{(p)} = \int E^p \, n_{i\alpha}(E) \, dE = \langle i\alpha | \hat{H}^p | i\alpha \rangle \tag{7}$$

which can be rewritten as

$$\mu_{i\alpha}^{(p)} = \sum_{j_1\beta_1 \ldots j_{p-1}\beta_{p-1}} H_{i\alpha,j_1\beta_1} H_{j_1\beta_1,j_2\beta_2} \ldots H_{j_{p-1}\beta_{p-1},i\alpha}. \tag{8}$$

Here the p-th moment is given as the sum over all bonding paths of length p that start and finish on the same atom i and orbital $|i\alpha\rangle$. We can also interpret this equation as a process of hopping on the lattice along closed paths of length p, where $H_{i\alpha,j\beta}$ describes the hop between orbital $|i\alpha\rangle$ and orbital $|j\beta\rangle$. The first moment consists of hops on a single site, the second of hops to the nearest neighbors and back, and so on. This is the key point since it shows a simple connection between the local bonding of an atom and its electronic structure, and provides thus an insight into the nature of cohesion and the structural stability.

Another crucial advancement in the work of Pettifor and Aoki [35,36] was the evaluation of the inter-site Green's function matrix elements in terms of the derivatives of the on-site Green's function matrix elements with respect to the moments. The most important result of this derivation is that these derivatives can be expressed entirely in terms of the recursion coefficients a_i and b_i. This leads to the final general formula for the bond order in the form of a multi-atom expansion which depends in a well defined way on the local environment about atoms.

σ bond order

For the derivation of the analytic formula for the σ bond order in the case of sp-valent systems with half full bands Pettifor and Oleinik [17] have taken the

BOP theory to four recursion levels in Eq. (6). In this way the true eigenspectrum is approximated by four poles or delta functions with non-zero recursion coefficients in Eq. (6) for $n < 4$. Furthermore, under the assumption that there are no odd-membered rings of atoms present, all odd moments are zero and, consequently, $a_n = 0$ for all n. The resultant formula for the bond order for a half-filled eigenspectrum in this so-called symmetric four-level approximation is then given by

$$\Theta_{ij,\sigma}^{(4Z)} = \left\{ \frac{1 + \dfrac{\hat{b}_2^2 - (\hat{b}_1^2 - 1) - \Re_{4\sigma}^{ij}}{(\hat{b}_1 + \hat{b}_3)\hat{b}_3}}{\sqrt{1 + \dfrac{\hat{b}_2^2}{(\hat{b}_1 + \hat{b}_3)^2}}} \right\} \frac{1}{\hat{b}_1} \tag{9}$$

where $\hat{b}_n = b_n/|\beta_\sigma|$ for $n = 1, 2, 3$ are the Lanczos recursion coefficients normalized by the β_σ bond integral (see Sec. 3.3) of the $i-j$ bond. The ring term $\Re_{4\sigma}^{ij}$ has been included later in the numerator [19] to account for four-member ring contributions which are important in close-packed structures.

The recursion coefficients $\hat{b}_1$ and $\hat{b}_2$ can be written explicitly in terms of the hopping paths of lengths two and four within the local atomic environment around the bond [37,15]:

$$\hat{b}_1^2 = 1 + \Phi_{2\sigma} \tag{10}$$

$$\hat{b}_1^2 \hat{b}_2^2 = (\hat{b}_1^2 - 1) - (\hat{b}_1^2 - 1)^2 + \Phi_{4\sigma} + \Re_{4\sigma}. \tag{11}$$

The recursion coefficient $\hat{b}_3$ is too complicated to be evaluated in an efficient way, and it is necessary to explore simplifying approximations. Pettifor and Oleinik have found a simplifying procedure by constraining the poles of the off-diagonal Green's function to be the same as those of the diagonal Green's function. This requirement allows for a derivation of an expression for $\hat{b}_3$ in terms of $\hat{b}_1$, $\hat{b}_2$ and additional ring terms, and it leads to the following expression for the constrained value of $\hat{b}_3$:

$$\hat{b}_3^2 = [(\hat{b}_2^2 - \Re_{4\sigma}^{ij}) - (\Phi_{2\sigma} - \Phi_{2\sigma}^i \Phi_{2\sigma}^j) + \Delta\Re^{ij}]/\Phi_{2\sigma} \tag{12}$$

The second-moment two-hop contribution $\Phi_{2\sigma}^i$, the fourth-moment four-hop contribution $\Phi_{4\sigma}^i$ and the interference three-hop contribution $\Re_{4\sigma}^{ij}$ in the above equations are schematically shown in Fig. 2. Mathematically these contributions are given by

$$\Phi_{2\sigma}^i = \sum_{k \neq i,j} [g_\sigma(\theta_{jik})]^2 \hat{\beta}_\sigma^2(R_{ik}) \tag{13}$$

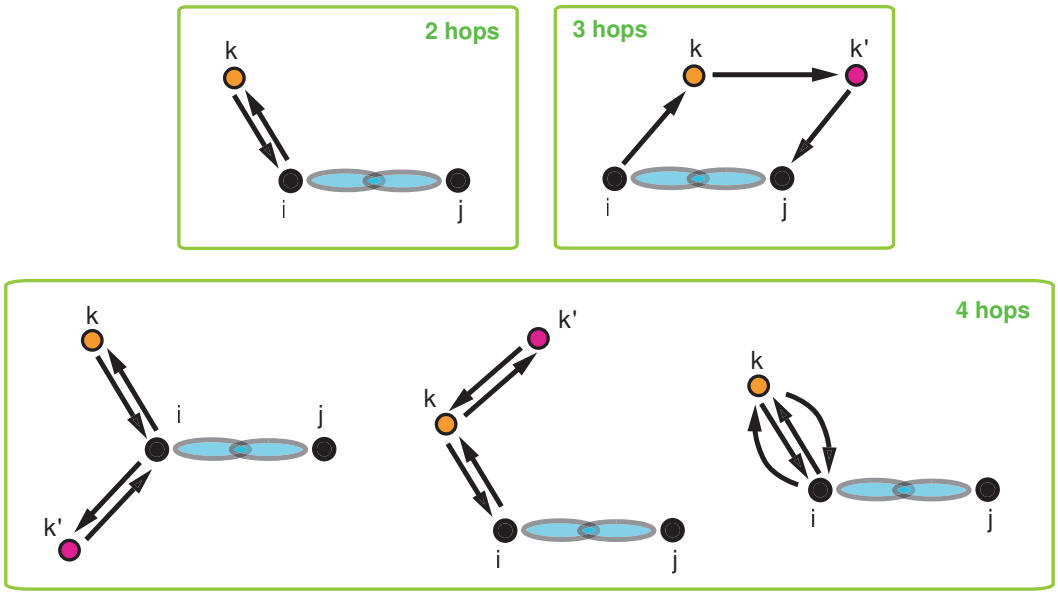

Fig. 2. Schematic diagrams of hopping paths of length 2, 3 and 4 which determine the σ bond order of the $i-j$ bond.

$$\begin{aligned}\Phi^{i}_{4\sigma} = & \sum_{k\neq i,j} [g_\sigma(\theta_{jik})]^2 \hat{\beta}^4_\sigma(R_{ik}) \\ & + \sum_{\substack{k,k'\neq i,j \\ k\neq k'}} g_\sigma(\theta_{jik}) g_\sigma(\theta_{kik'}) g_\sigma(\theta_{k'ij}) \hat{\beta}^2_\sigma(R_{ik}) \hat{\beta}^2_\sigma(R_{ik'}) \\ & + \sum_{\substack{k,k'\neq i,j \\ k\neq k'}} [g_\sigma(\theta_{jik}) g_\sigma(\theta_{ikk'})]^2 \hat{\beta}^2_\sigma(R_{ik}) \hat{\beta}^2_\sigma(R_{kk'})\end{aligned} \tag{14}$$

$$\begin{aligned}\Re^{ij}_{4\sigma} = & \sum_{\substack{k,k'\neq i,j \\ k\neq k'}} g_\sigma(\theta_{jik}) g_\sigma(\theta_{ikk'}) g_\sigma(\theta_{kk'j}) g_\sigma(\theta_{k'ji}) \\ & \times \hat{\beta}_\sigma(R_{ik}) \hat{\beta}_\sigma(R_{kk'}) \hat{\beta}_\sigma(R_{k'j})\end{aligned} \tag{15}$$

with the normalized bond integrals $\hat{\beta}_\sigma(R_{kk'}) = \beta_\sigma(R_{kk'})/\beta_\sigma(R_{ij})$ and $\Phi_{n\sigma} = \frac{1}{2}(\Phi^i_{n\sigma} + \Phi^j_{n\sigma})$. The angular function $g_\sigma(\theta_{jik})$ depends on the angle θ_{jik} subtended between the bonds ij and ik as well as on the type of the atom i. It is given by $g^H_\sigma(\theta) = 1$ for hydrogen, and $g^C_\sigma(\theta) = [(1-p_\sigma) + p_\sigma \cos\theta]$ for carbon, where $p_\sigma = \mathrm{pp}\sigma/(|\mathrm{ss}\sigma| + \mathrm{pp}\sigma)$ is the ratio of C–C bond integrals (see next section for details).

Substituting Eqs. (10), (11) and (12) into Eq. (9) and neglecting some higher order terms leads to an expression for the bond order derived in Ref. [19], namely

$$\Theta^{(BOP)}_{ij,\sigma} = \frac{1}{\sqrt{1 + \dfrac{2\Phi_{2\sigma} + \Re^{ij}_{4\sigma} + \widetilde{\Phi}^i_{2\sigma}\widetilde{\Phi}^j_{2\sigma}(2 + \widetilde{\Delta\Phi}_{4\sigma})}{(1 + \widetilde{\Delta\Phi}^2_{4\sigma})^2}}} \tag{16}$$

where

$$\widetilde{\Phi}^i_{2\sigma}\widetilde{\Phi}^j_{2\sigma} = \Phi^i_{2\sigma}\Phi^j_{2\sigma}/\sqrt{\Delta\Phi_{4\sigma} + \Phi^i_{2\sigma}\Phi^j_{2\sigma}} \tag{17}$$

$$\widetilde{\Delta\Phi}^2_{4\sigma} = \Delta\Phi_{4\sigma}/\sqrt{\Delta\Phi_{4\sigma} + \Phi^i_{2\sigma}\Phi^j_{2\sigma}} \tag{18}$$

with

$$\Delta\Phi_{4\sigma} = \frac{\Phi_{4\sigma} - \frac{1}{2}[(\Phi^i_{2\sigma})^2 + (\Phi^j_{2\sigma})^2]}{\Phi_{2\sigma}}. \tag{19}$$

It has been shown [19] that Eq. (16) gives excellent results for both open and close-packed carbon phases under the assumption that the valence s and p electrons take identical on-site energy levels. However, in the case of carbon where the atomic sp energy level separation, $\delta^C = (\epsilon^C_p - \epsilon^C_s) = 6.7$ eV, is rather large, it is necessary to account for this non-negligible difference. Following Ref. [18] we therefore modified Eq. (16) to a form

$$\Theta^{(BOP)}_{ij,\sigma} = \frac{1}{\sqrt{1 + \dfrac{2\Phi_{2\sigma} + \hat{\delta}^2_2 + \Re^{ij}_{4\sigma} + \widetilde{\Phi}^i_{2\sigma}\widetilde{\Phi}^j_{2\sigma}(2 + \widetilde{\Delta\Phi}_{4\sigma})}{(1 + \widetilde{\Delta\Phi}^2_{4\sigma})^2}}} \tag{20}$$

where $\hat{\delta}^2_2$ is defined as

$$\hat{\delta}^2_2 = (1 + \Phi_{2\sigma})\hat{\delta}^2 \tag{21}$$

with

$$\hat{\delta}^2 = \tfrac{1}{2}[(\delta^i)^2 + (\delta^j)^2][4p_\sigma(1 - p_\sigma)]/[\beta_\sigma(R_{ij})]^2. \tag{22}$$

δ^i and δ^j are the sp energy splittings of atoms i and j, respectively (i.e. $\delta^H = 0$ and $\delta^C = 6.7\,\mathrm{eV}$). Eq. (22) has been derived in earlier papers of Pettifor and coworkers [15,38] and the delta term $\hat{\delta}^2$ has been included in the bond order expression in Ref. [18]. The origin of this term can be traced back to the recursion coefficient $\hat{b}_1$. The explicit form of $\hat{b}_1$ for non-zero sp splitting has been derived in Ref. [15] as

$$\hat{b}^2_1 = 1 + \Phi_{2\sigma} + \hat{\delta}^2. \tag{23}$$

A rigorous derivation of the σ bond order with this expression leads unfortunately to a too complicated formula and we therefore retained only a simplified form of $\hat{\delta}^2_2$ with a second order term which incorporates the environmental dependence via the second-moment term $\Phi_{2\sigma}$. The inclusion of the $\hat{\delta}^2_2$ term in Eq. (20) is a very important generalization. Through this term the bond order depends explicitly on the sp splitting and provides thus a correct description of the loss of covalent bonding due to the difference in the s and p on-site energies. In the case of the carbon dimer it reduces to the correct limit of $1/\sqrt{1 + \hat{\delta}^2}$ and not to the value of unity which would result from Eq. (16).

Eq. (20) has been used in all calculations of the σ bond order in the current paper. It will be shown in the next section that the presence of the $\hat{\delta}^2_2$ term in the bond order formula is essential for a correct description of bonding

under non-equilibrium conditions such as during chemical reactions or within amorphous structures.

π bond order

The incorporation of the π bond description in the ABOP formalism is an important improvement over the Tersoff-Brenner potentials, since neither of these potentials includes an appropriate π bond contribution. The neglect of π bonding leads to several problems such as overbinding of radicals, incorrect treatment of conjugacy and underestimation of rotation barriers.

For the derivation of the π bond order the BOP theory has been taken to two levels of recursion in the continued fraction (Eq. (6)). Furthermore, by constraining the poles of G_{ij} a constrained value of $\hat{b}_2 = \sqrt{\hat{b}_1^2 - 1}$ is obtained within the three-level recursion formalism [19]. This approximation thus describes exactly saturated π bonds in two-level C_2, C_2H_2 and C_2H_4 molecules, and predicts values for the conjugate bond orders in graphite and benzene within 10% of the OTB values. The analytic expression for the π bond order then takes the form

$$\Theta_{ij,\pi}^{(BOP)} = \frac{1}{\sqrt{1 + \Phi_{2\pi} + \Phi_{4\pi}^{1/2}}} + \frac{1}{\sqrt{1 + \Phi_{2\pi} - \Phi_{4\pi}^{1/2}}} \tag{24}$$

where the two-hop contribution is given as

$$\begin{aligned}\Phi_{2\pi}^{i} = \sum_{k \neq i,j} \{ & \sin^2\theta_{jik}\, p_\sigma [\hat{\beta}_\sigma^{C\kappa}(R_{ik})]^2 \\ & + (1 + \cos^2\theta_{jik}) [\hat{\beta}_\pi^{CC}(R_{ik})]^2 \delta_{\kappa C}\},\end{aligned} \tag{25}$$

and the four-hop contribution as

$$\begin{aligned}\Phi_{4\pi}^{i} = \tfrac{1}{2} \sum_{k,k' \neq i,j} & (\sin^2\theta_{jik} \sin^2\theta_{jik'} + \sin^2\theta_{jik} \sin^2\theta_{ijk'}) \\ & \tilde{\beta}_{ik}^2 \tilde{\beta}_{ik'}^2 \cos 2(\phi_k - \phi_{k'})\end{aligned} \tag{26}$$

with

$$\tilde{\beta}_{ik}^2 = p_\sigma [\hat{\beta}_\sigma^{C\kappa}(R_{ik})]^2 - [\hat{\beta}_\pi^{CC}(R_{ik})]^2 \delta_{\kappa C}. \tag{27}$$

In the above formulas the capped integrals have been normalized by the π bond integral $\beta_\pi^{CC}(R_{ij})$ and not by the σ bond integral as in the case of the σ bond order (cf text following Eq. (15) above). The superscript κ refers to the nature of atomic species (i.e. H or C) and the Kronecker delta $\delta_{\kappa C}$ ensures that there are no π bond contributions for C–H bonds.

There is one further approximation to be mentioned when going from the OTB model to ABOP for the hydrocarbon system. The C–C σ bond in the conventional two-center OTB model is described by three bond integrals: ssσ, spσ and ppσ [30]. Consequently, there is not a single bond order which characterizes this bond but three separate quantities. In order to obtain a single scalar bond order Θ_σ it is convenient to restrict the spσ bond integral to be the geometric mean of |ssσ| and ppσ [37]. The three OTB bond integrals are thus reduced to two quantities: a single ABOP bond integral β_σ and a parameter p_σ which gives the relative amount of s and p orbitals in the bonding hybrid orbital [39]. The relations between the TB and ABOP bond integrals for the C–C bond can be then written as

$$\left.\begin{array}{c} \mathrm{ss}\sigma^{CC} \\ \mathrm{sp}\sigma^{CC} \\ \mathrm{pp}\sigma^{CC} \end{array}\right\} = \left\{\begin{array}{c} -(1-p_\sigma) \\ \sqrt{p_\sigma(1-p_\sigma)} \\ p_\sigma \end{array}\right\} \beta_\sigma^{CC}(R). \tag{28}$$

Similarly, the C–H bond integrals can be written in the form

$$\left.\begin{array}{c} \mathrm{ss}\sigma^{CH} \\ \mathrm{sp}\sigma^{CH} \end{array}\right\} = \left\{\begin{array}{c} -\sqrt{1-p_\sigma} \\ \sqrt{p_\sigma} \end{array}\right\} \beta_\sigma^{CH}(R) \tag{29}$$

where it was assumed that $(\mathrm{sp}\sigma/|\mathrm{ss}\sigma|)^{CH} = (\mathrm{sp}\sigma/|\mathrm{ss}\sigma|)^{CC} = \sqrt{p_\sigma/(1-p_\sigma)}$. It was shown in Ref. [40] that the constraint equations (28) and (29) are excellent approximations for the hydrocarbon system within the well known and widely used OTB parameterization of Xu et al. [41] and Davidson and Pickett [42]. This orthogonal TB model has provided many valuable results but, unfortunately, it also suffers from several weaknesses. It is rather short ranged and with the cut-off distance for C–C interactions of only 2.6 Å it cannot, for example, describe correctly the interlayer graphite spacing, diamond-graphite phase transformation, or some dissociation reactions. The parameterization also underestimates the magnitude of the π bond integral. This leads to a prediction of the wrong electronic ground-state configuration for the carbon dimer as well as unsatisfactory electronic band structures of closed packed bulk phases. Furthermore, it was shown recently [22] that this model underestimates the sp^3 fraction in amorphous carbon films.

In the current work we do not aim at the improvement of the original OTB parameterization. [1] Instead, we use this extensively tested model and compare it to its coarse-grained offspring – the ABOP. It is important to stress that

[1] The OTB parameterization used in this work is summarized in Ref. [43]. We were

within the reduced OTB model (Eqs. (28) and (29)) the OTB and ABOP parameterizations are fully equivalent and, ideally, the ABOP and OTB results should coincide. The differences between predictions of these two models are therefore solely due to the approximations implemented during the coarse-graining process. How ABOP holds its grounds is the subject of the following section.

4 ABOP vs. OTB

Unlimited transferability of empirical potentials is the holy grail of atomistic simulations. With potentials like Tersoff [12], Brenner [13], EDIP [44] or ReaxFF [45], which are to a greater or lesser extent based on empirical rather than on quantum-mechanical concepts, there is always a significant risk of failure when these models are applied to situations far from their proven fitting pools. When problems appear there is unfortunately only a limited number of possible cures. Obvious ones are the extension of the fitting database to include the problematic area and modification of model parameters, or perhaps, an addition of further terms to correct for the discrepancy. The bond-order approach however enables a general and systematic derivation of the interatomic potential based on the topology of bonding and quantum mechanical concepts of chemical bonds. Not only is it extremely appealing to have the interatomic potential rigorously derived from higher-level theory, but it also becomes much easier to trace back the origins of eventual problems to approximations made during derivation. Furthermore, since ABOPs are based on the OTB model, fitting may not be necessary if there is a reliable OTB parameterization available. Even if a new parameterization is needed, the only input parameters for the crucial bonding part of the potential are the Slater-Koster bond integrals which have a physically transparent interpretation. This is in a sharp contrast to some of the methods mentioned above which require close to hundred parameters and elaborate fitting strategies.

In the following we present calculations for crystalline and amorphous bulk phases as well as for molecules and small clusters studied in parallel by the reduced OTB model and ABOP. The main focus of these test calculations is on the key quantity – the bond order – since it immediately reveals the strengths as well as the limitations of ABOP.

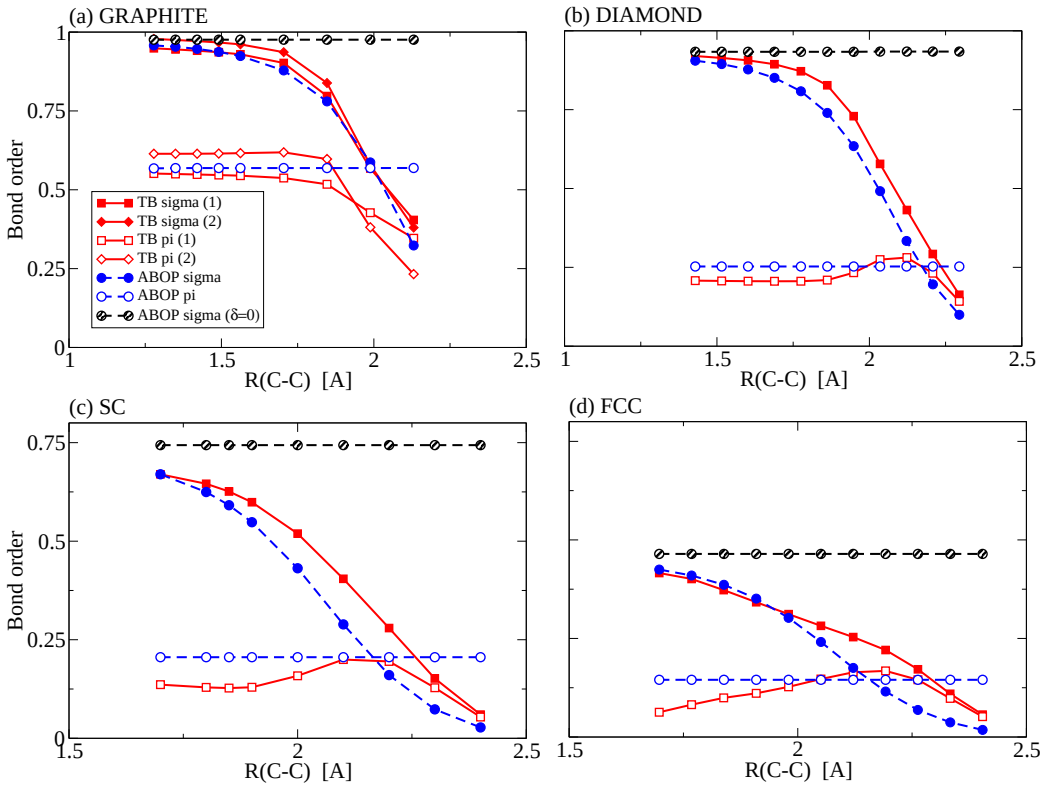

Fig. 3. Comparison of OTB and ABOP results of the σ (using both Eq. (20) and Eq. (16)) and π bond order (using Eq. (24)) for graphite, diamond, sc and fcc structures as a function of C–C interatomic distance. (There are two sets of TB data for the graphite structure due to two inequivalent atoms.)

4.1 Crystalline carbon phases

For atomistic simulations of solids the first requirement is a correct description of equilibrium as well as alternative crystalline phases. We calculated energy versus volume curves for graphite, diamond, simple cubic, body-centered cubic (bcc) and face-centered cubic (fcc) structures. The coordination number in these structures increases from 3 to 12, and thus these calculation provide information about the bonding variation from fully saturated covalent bonds in graphite and diamond to unsaturated bonds in close-packed structures. Instead of showing the usual dependence of the total energy as a function of volume we focus in our analysis on the change of the σ and π bond orders. The results are shown in Fig. 3. As we stressed in the previous section, the non-negligible difference in the carbon s and p on-site energies has a profound influence on the behavior of the σ bond order. This is clearly visible from the data in Fig. 3 which include σ bond order values calculated both by Eq. (20) and by Eq. (16) which does not contain the $\hat{\delta}_2^2$ term. While Eq. (20)

forced to refit the repulsive terms in order to avoid nonphysical attractions at very short distancies of the original many-body repulsive functional forms.

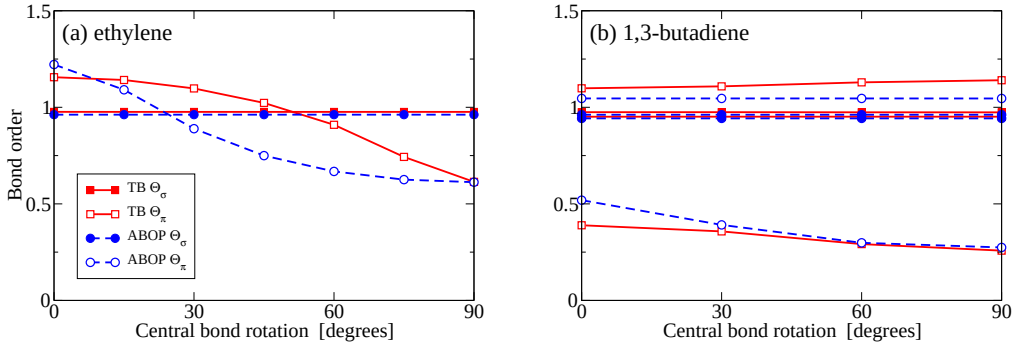

Fig. 4. Change of bond orders for the rotation around the central C=C bond in ethylene (a) and around the central C–C bond in 1,3-butadiene.

reproduces very well both the magnitude and the decay of Θ_σ with increasing C–C bond length, the neglect of the sp splitting in the bond order expression leads to a constant value of the σ bond order. The error introduced in this way increases with increasing bond length and leads to an overestimation of the σ bond order by Eq. (16) for longer bonds. Even though the absolute error in the bond energy is damped down by decreasing bond integrals, we will demonstrate in the following that the neglect of the $\hat{\delta}_2^2$ term leads to incorrect configurations of small carbon clusters and to a significant overcoordination of atoms in amorphous structures. In the case of the π bond order the OTB model predicts only a weak dependence on the bond length which justifies the neglect of the sp splitting in the ABOP π bond order.

4.2 Molecules and clusters

Results of ABOP and OTB calculations for various hydrocarbon molecules in their ground-state geometries have been compared already in the original papers of Pettifor and Oleinik [40,18]. It has been shown that ABOP reproduces the OTB values excellently except for extreme cases such as CH and CH_2 radicals where spin polarization has to be taken into account. ABOP also handles correctly the radical formation. The ethyl radical (C_2H_5) remains to be essentially single bonded after H abstraction from ethane, unlike in the Tersoff potential which predicts the carbon bond to be an average of the single and double bond. We have performed additional tests for a wider class of molecules containing single, double, triple and conjugated bonds in different local arrangements to extend the testing. The average root mean square errors in our calculations for different classes of molecules did not exceed 0.15 eV/atom. Details of these tests will be presented elsewhere.

In addition to the dependence of the bond order on the bond stretching another important property is the resistance of double, triple and conjugated bonds to rotations. In a typical example of ethylene the conventional saturated π

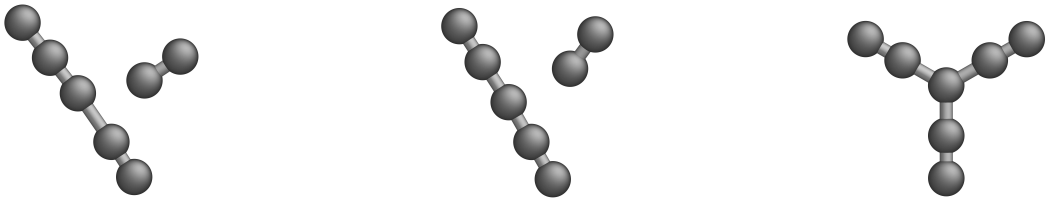

(a) (b) (c)

Fig. 5. Configurations of the C_7 cluster relaxed with ABOP using (a) $\Theta_\sigma^{\delta_0}$, (b) $\Theta_\sigma^{\delta_1}$ and (c) $\Theta_\sigma^{\delta_2}$ bond orders.

bond is broken under rotation which requires an energy of about 3 eV. ABOP and OTB give barrier heights of 3.4 eV and 3.6 eV, respectively, which are in a good agreement with DFT calculations [17].

A more interesting case of a rotation barrier can be found in the class of conjugated dienes such as 1,3-butadiene. This molecule contains two carbon double bonds separated by a single bond. In such an arrangement the π electrons of the two double bonds lower their energy by delocalization along the carbon chain and form a conjugated bond. As a result the single bond between the two conjugated double bonds is strengthened and also shortened due to the acquired π character. Since neither Tersoff nor original Brenner potentials contain appropriate descriptions of double and conjugated bonds they predict no rotation barrier around the central C–C bond in 1,3-butadiene or, in general, for any conjugated bond. The variation of bond orders during twisting of ethylene and 1,3-butadiene is shown in Fig. 4. In both cases the OTB and ABOP σ bond orders agree almost perfectly and remain constant while the π bond orders decrease significantly as the molecules are twisted. For 1,3-butadiene there are two sets of values for the π bond order corresponding to the double conjugated bond with $\Theta_\pi \approx 1.05$ and the single conjugated bond with $\Theta_\pi \approx 0.45$. At the rotation angle of 90° the conjugation is essentially removed and the central C–C bond becomes an ordinary single bond.

Since our ultimate goal is the simulation of amorphous films grown by deposition of molecules on surfaces, it is crucial to verify that the ABOP potential describes well also non-equilibrium configurations. The amorphous a-C or a-C:H films are usually prepared by plasma deposition of various hydrocarbon molecules. The local atomic structure of the films is determined by breaking, stretching and twisting of bonds induced by the impacting molecules. Our initial simulations of a-C:H film growth using original expressions for the σ and π bond orders from Ref. [19] showed promising results but at the same time we observed an nonphysical accumulation of overcoordinated atoms with increasing deposition time. In order to determine the origin of this discrepancy we attempted to reduce the complexity of the problem and to analyze first several simple amorphous structures. This was done by picking up random configurations of small carbon clusters out of an amorphous network and

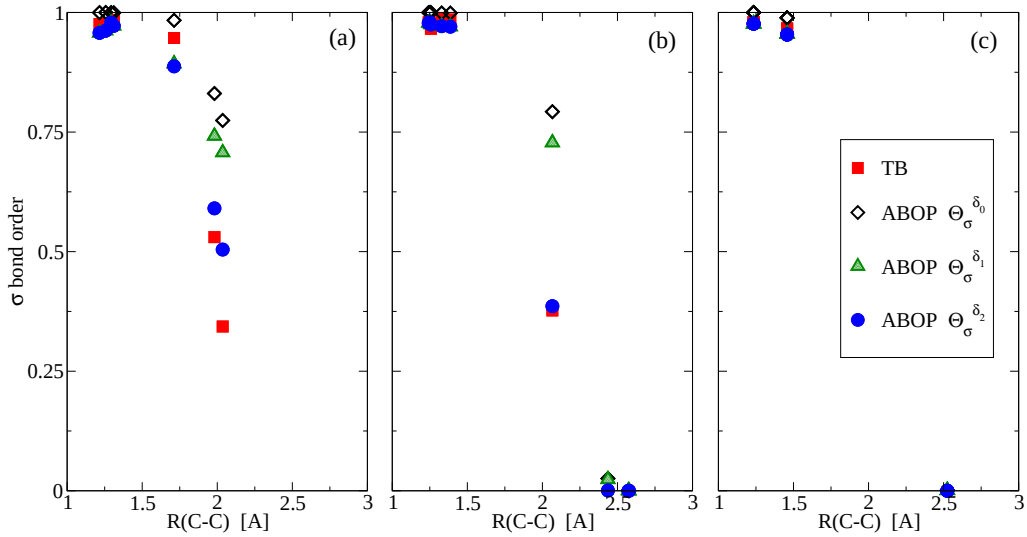

Fig. 6. Comparison of the $\Theta_\sigma^{\delta_0}$, $\Theta_\sigma^{\delta_1}$ and $\Theta_\sigma^{\delta_2}$ bond orders for the C_7 clusters (panels (a), (b) and (c) correspond to clusters shown in Fig. 5(a), (b) and (c), respectively).

comparing the OTB and ABOP results for their equilibrium geometries.

An example of one such calculation for a C_7 cluster is shown in Fig. 5. The three displayed structures have been relaxed from the same starting configuration using ABOP with three different approximations for the σ bond order. For clarity we will designate in the following these three σ bond orders with the acronyms $\Theta_\sigma^{\delta_0}$, $\Theta_\sigma^{\delta_1}$ and $\Theta_\sigma^{\delta_2}$ according to evaluation of the $\hat{\delta}_2^2$ term in Eq. (21) which reflects the sp splitting of the on-site energies. The bond orders were calculated as

$$\text{for} \quad \Theta_\sigma^{\delta_0}: \qquad \hat{\delta}_2^2 = 0 \tag{30}$$

$$\text{for} \quad \Theta_\sigma^{\delta_1}: \qquad \hat{\delta}_2^2 = \hat{\delta}^2 \tag{31}$$

$$\text{for} \quad \Theta_\sigma^{\delta_2}: \qquad \hat{\delta}_2^2 = \hat{\delta}^2 + \Phi_{2\sigma}\hat{\delta}^2. \tag{32}$$

Eq. (30) corresponds to a neglect of the sp splitting in the σ bond order expression and $\Theta_\sigma^{\delta_0}$ is therefore equivalent to the σ bond order of Pettifor and Oleinik in Ref. [19] (i.e. Eq. (16)). This expression, which was also used in our initial film growth simulations, leads to the equilibrium structure of the C_7 cluster shown in Fig. 5(a). Eq. (31) includes the sp splitting in the simplest possible way via the simple $\hat{\delta}^2$ term [18]. Using this approximation the C_7 cluster relaxes to the structure in Fig. 5(b). Finally, the symmetric tri-star configuration in Fig. 5(c) is the equilibrium structure obtained by ABOP with the $\Theta_\sigma^{\delta_2}$ bond order evaluated according to Eq. (32) which includes the second order contribution $\Phi_{2\sigma}\hat{\delta}^2$. The star geometry is also the equilibrium structure predicted by OTB. The three structures in Fig. 5 are clearly related and the configuration (b) can be viewed as an intermediate state between (a) and (c). The analysis of individual bonds in the three structures in terms of the σ bond order reveals how sensitive is the final configuration to the correct description

of the sp splitting in the bond order expression. The comparison of OTB bond orders with $\Theta_\sigma^{\delta_0}$, $\Theta_\sigma^{\delta_1}$ and $\Theta_\sigma^{\delta_2}$ bond orders for all bonds in the molecules from Fig. 5 is shown in Fig. 6. The $\Theta_\sigma^{\delta_0}$, $\Theta_\sigma^{\delta_1}$ and $\Theta_\sigma^{\delta_2}$ values are marked by diamonds, triangles and circles, respectively. The calculations show that the "equilibrium" C–C bonds with bond lengths up to 1.5 Å are described correctly by all three ABOP bond orders, reaching values close to one in agreement with OTB. This is an expected result established already in the original papers as well as in our additional studies of hydrocarbon molecules in their ground-state geometries. However, for longer bonds of about 2.0 Å, which correspond to interactions between the long linear chain and the carbon dimer in Fig. 5(a) and (b), the agreement between OTB and ABOP improves dramatically as the description of the sp splitting improves from Eq. (30) via Eq. (31) to Eq. (32). In the case of inter-chain bonds in the intermediate structure in Fig. 6(b), the $\Theta_\sigma^{\delta_2}$ bond order coincides almost perfectly with the OTB value while $\Theta_\sigma^{\delta_0}$ and $\Theta_\sigma^{\delta_1}$ give values more than twice as large. Such large errors in bond orders lead to an absolute increase of the bond energy for these inter-chain bonds and to an nonphysical stabilization of structures in Fig. 6(a) and (b) when $\Theta_\sigma^{\delta_0}$ and $\Theta_\sigma^{\delta_1}$ bond orders are used. We have found similar nonphysical behavior in other small carbon clusters as well as in larger amorphous structures shown in the next section. In general, the errors in bond orders and bond energies with $\Theta_\sigma^{\delta_0}$ and $\Theta_\sigma^{\delta_1}$ bond orders reach a maximum for bonds with lengths between 1.8 and 2.0 Å. The insufficient treatment of the sp splitting in these σ bond orders is therefore directly responsible for overcoordinations in amorphous structures which will be discussed next.

4.3 Amorphous phases

Amorphous structures present one of the most stringent tests for interatomic potentials. To investigate the behavior of ABOP for amorphous environments we performed liquid-quench simulations for a pure carbon system. Same calculations have been performed with the non-orthogonal tight-binding (NOTB) and OTB models as well as with two variations of Brenner potentials with different values of cut-off radii. Furthermore, we compared our results with data from a recent theoretical study of Marks et al. [22].

The amorphous carbon structure was prepared in an often used manner, by melting an unstable simple cubic lattice containing 125 atoms with a density of 2.9 g/cm^3. After spontaneous melting the structure was equilibrated at 5000 K for 1 ps with a time step of 0.05 fs. The radial distribution function (RDF) of the resulting liquid is plotted in Fig. 7(a). In this picture we compare again results obtained with $\Theta_\sigma^{\delta_0}$, $\Theta_\sigma^{\delta_1}$ and $\Theta_\sigma^{\delta_2}$ bond orders. The difference between RDF curves computed with different bond orders is striking. Both $\Theta_\sigma^{\delta_0}$ and $\Theta_\sigma^{\delta_1}$ yield completely wrong structures of the liquid and only $\Theta_\sigma^{\delta_2}$

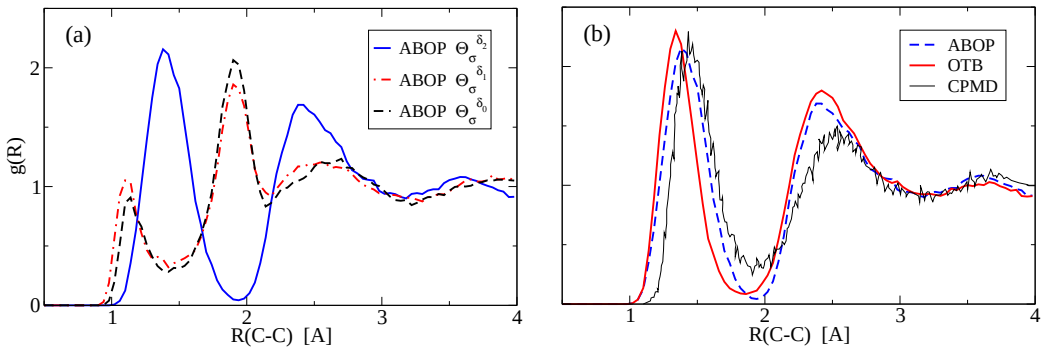

Fig. 7. Comparison of radial distribution functions g(R) for 2.9 g/cm^3 liquid carbon (at 5000 K) simulated by (a) ABOP with $\Theta_\sigma^{\delta_0}$, $\Theta_\sigma^{\delta_1}$ and $\Theta_\sigma^{\delta_2}$ bond orders and (b) ABOP ($\Theta_\sigma^{\delta_2}$), OTB and CPMD from Ref. [22].

is able to reproduce correctly the liquid behavior. This result is consistent with the previous findings but the deficiencies of the $\Theta_\sigma^{\delta_0}$ and $\Theta_\sigma^{\delta_1}$ bond orders are most pronounced here. The tendency of $\Theta_\sigma^{\delta_0}$ and $\Theta_\sigma^{\delta_1}$ to overcoordination due to overestimated bond orders in longer bonds leads to the nonphysical liquid structure dominated by bonds of lengths 1.8-2.0 Å. The description of the liquid state therefore strongly correlates with the description of the sp splitting. Fig. 7(b) shows a comparison of RDF curves from ABOP and OTB with the Car-Parinello first-principles molecular dynamics (CPMD) results of Marks et al. [46]. ABOP with the $\Theta_\sigma^{\delta_2}$ bond order agrees well with the TB distribution but both methods show a small offset in the position of the first peak with respect to CPMD. The reasons for this discrepancy are discussed below.

After equilibration, the carbon liquid was cooled down to room temperature during 14 ps. Three cooling regimes with the cooling rates of 1000 K/ps, 250 K/ps and 100 K/ps were used in temperature intervals 5000-2000 K, 2000-1000 K and 1000-300 K, respectively. Comparison of reduced radial distribution functions of the quenched samples with those of other methods of Ref. [22] is displayed in Fig. 8(a). ABOP ($\Theta_\sigma^{\delta_2}$) again agrees well with OTB but both methods as well as the original Brenner potential underestimate significantly the sp^3 fraction compared to CPMD and experiment. It was suggested by Marks et al. [22] that the reason for this behavior is the short range of the C–C interactions in these potentials which leads to high-density graphitic structures. The modified Brenner potential of Jäger and Albe [21] predicts the sp^3 fractions greater than 80%, but this improvement occurs at the expense of a large number of nonphysical metastable distances intermediate between the first and second neighbors (spurious peaks above 2 Å in the lowest panel of Fig. 8(a)) and an increase of five-fold coordinated atoms. The EDIP model which was specifically constructed for simulations of amorphous carbon gives a good overall agreement with CPMD and NOTB and seem to be currently the most reliable empirical scheme for description of a-C networks.

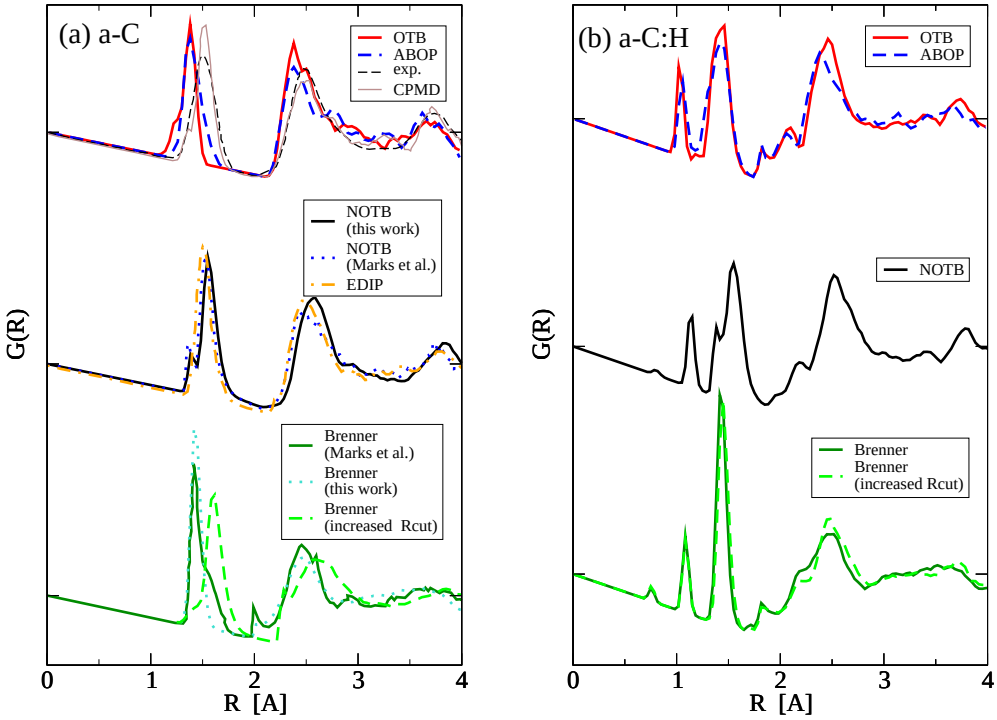

Fig. 8. Comparison of reduced radial distribution functions produced by different methods for (a) a-C sample with the density of 2.9 g/cm^3 and (b) a-C:H sample with the density of 2.5 g/cm^3.

5 From a-C to to a-C:H

Going from simulations of pure a-C to simulations of hydrogenated amorphous carbon is not a trivial step. Depending on preparation conditions and hydrogen concentration a-C:H materials can vary from soft, low-density phases with polymer-like atomic structures to hard, diamond-like materials with a high content of C–C sp^3 bonds. Even though a-C:H films have important practical applications due to their diverse properties [20] there has been only a handful of theoretical studies of these systems [47–50]. Moreover, due to computational costs all these attempts have been restricted to small system sizes and rather unrealistic conditions and are therefore of limited practical use. The obvious reason for the missing theoretical involvement is a lack of reliable interatomic potentials. To our knowledge there are currently no other interatomic potentials available for the hydrocarbon system than ABOP, ReaxFF [45], and the Brenner potential and its extensions [51,52]. In this section we describe the first application of ABOP for the a-C:H system. We again have to bear in mind the limitations of the OTB parameterization which is used for ABOP as well. The results of our studies should be therefore considered as qualitative rather than quantitative and at this stage the calculations serve more as another benchmark of ABOP.

As in the case of a-C, we have performed a series of simulations of bulk a-

C:H samples at various densities. The calculations were done by four methods – original Brenner potential, Brenner potential with an increased cut-off of 2.25 Å, ABOP/OTB and NOTB. For ABOP calculations reported in this section we used only the $\Theta_\sigma^{\delta_2}$ bond order of Eq. (32) since the other two approximations were certain to yield wrong results as we have demonstrated above. The simulation blocks contained in all cases 215 atoms with 169 carbon and 46 hydrogen atoms. This corresponds to 21% hydrogen concentration which is close to the range of experimentally observed values for tetrahedral a-C:H thin films [20]. After an equilibration period of 1 ps at 5000 K the systems were quenched to room temperature with a cooling rate of 1000 K/ps. The properties of the a-C:H networks were then analyzed during a NVT molecular dynamics run at room temperature for additional 0.5 ps. The results of the analysis and the comparison with results of different methods are summarized in Figs. 8(b) and 9.

The reduced radial distribution functions for the quenched a-C:H samples with the density of 2.5 g/cm^3 (which is the highest experimentally observed density of a-C:H films [53]) are presented in Fig. 8(b). ABOP reproduces well OTB results and the RDF curves of both methods agree reasonably well with those of NOTB calculations but with a systematically lower sp^3/sp^2 ratio, similarly as in the a-C case. RDFs obtained with both Brenner's potentials deviate from those obtaine with the other three methods, and the Brenner potentials predict nearly pure graphitic structures. The influence of the cut-off radius on the behavior of Brenner's potentials is analyzed in detail below. RDFs for the a-C:H structures can be also easily compared with those of the a-C structures in Fig. 8(a). The most obvious difference between the a-C and a-C:H curves are additional peaks corresponding to C–H bonds. The most pronounced peak at 1.1 Å corresponds to first nearest neighbor C–H interactions. Other smaller peaks between 1.7 and 2.2 Å belong to correlations in the second coordination shell associated with H–C–H and C–C–H bonds. These small features are in a a good agreement with experimental observations [54].

Fig. 9(a) shows the variation of the sp^1, sp^2 and sp^3 content as a function of density from ABOP simulations. For the lowest density of 2.0 g/cm^3 the amorphous structure does hardly contain any sp^3 atoms and is composed almost fully of graphitic-like networks with a small fraction of sp^1 linear chains. As the density increases the sp^3/sp^2 ratio increases linearly and the networks at densities larger than 2.5 g/cm^3 are only mixtures of sp^2 and sp^3 atoms. Unlike in simulations with the original bond order expression (Eq. (16)), we have not detected any atoms with coordination numbers higher then four in these simulations.

Fig. 9(b) presents a comparison of sp^3 fractions obtained by the four different methods. The NOTB calculations yield a near-linear increase of the sp^3 content with the density in agreement with available experimental observations [53].

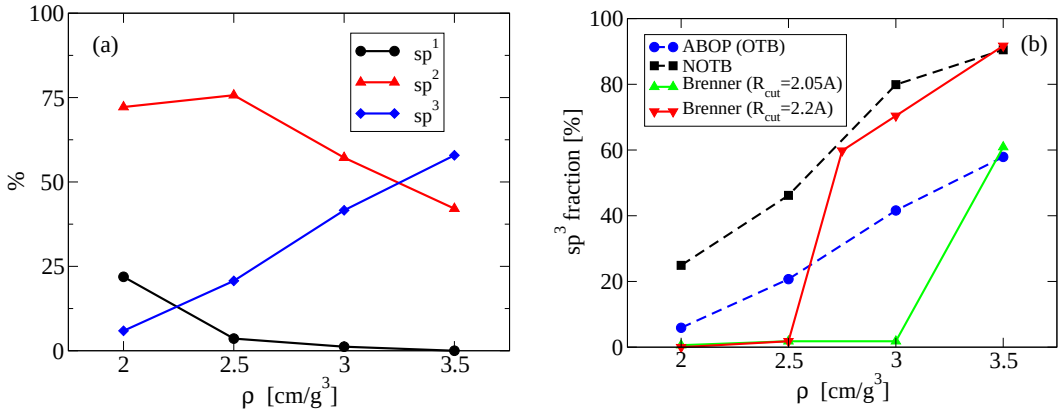

Fig. 9. (a) Comparison of carbon bonding in a-C:H samples of different density simulated by ABOP and (b) variation of sp^3 content predicted by ABOP, NOTB and two Brenner potentials with different cut-offs.

A similar linear correlation between the sp^3 concentration and the density, albeit with a lower sp^3 content like in the a-C case, is also obtained by the ABOP/OTB methods. In contrast, for Brenner potentials the sp^3 fraction is strongly dependent on the potential cut-off. The original parameterization with $R_{cut} = 2.0\,\text{Å}$ produces a negligible sp^3 content up to the density of 3.0 g/cm^3. For the density of 3.5 g/cm^3 the sp^3 fraction sharply increases to 60%. The Brenner potential with the cut-off radius increased to 2.25 Å shows a similar behavior but the abrupt transition to higher sp^3 content is shifted to a lower density of approximately 2.6 g/cm^3. This example clearly shows the danger of *ad hoc* variation of parameters in semiempirical models. By varying the interaction range of the potential (in this case the Brenner potential but the same procedure done for the Tersoff potential has given similar results [55]) one can achieve a better agreement with reality for a specific configuration but predictions of the model remain unchanged in other areas which were unaffected by the parameter modification (in this case the lower density structures).

Film growth simulations

Process of film growth by implantation of energetic ions brings further challenges to molecular dynamics simulations. Simulation blocks have to contain more than thousand atoms to avoid boundary effects during a cascade of events after ion implantation, and simulation times usually exceed million of steps to reach the steady-state growth. Thus the model describing interatomic interactions in film growth simulations has to provide not only an excellent transferability but also a good efficiency. Recently, Marks et al. [56] have performed first simulations of a-C film growth using the EDIP model. These calculations reproduced the dependence of the sp^3 fraction on the energy of deposited ions but the grown films contained a high sp^3 content already for

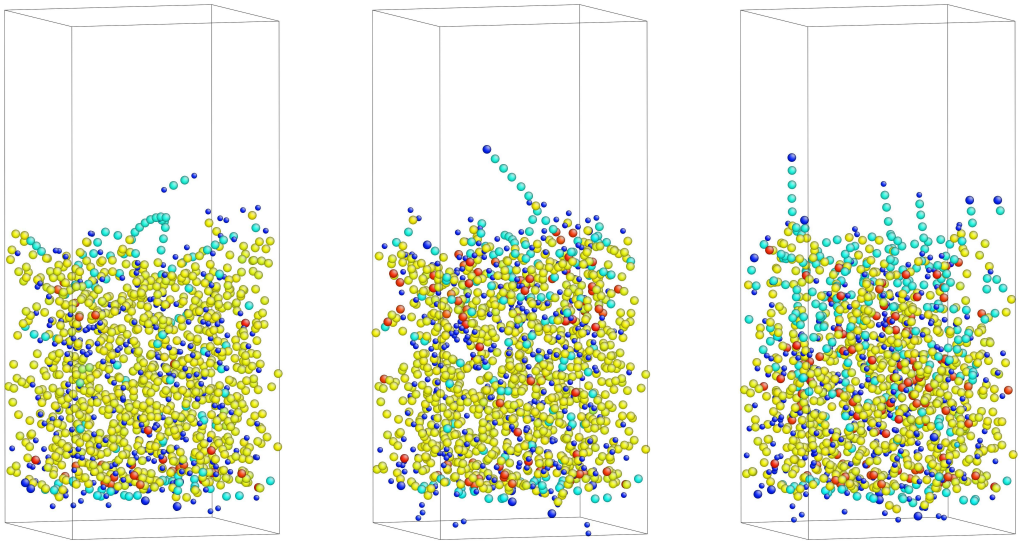

(a) (b) (c)

Fig. 10. Atomic structures of the simulated a-C:H films; (a) initial structure, (b) and (c) final structures after deposition of 50 acetylene molecules with energies of 25 and 100 eV per carbon atom, respectively.

ion energies of less than 10 eV in disagreement with experiment. Furthermore, the EDIP model is limited to simulations of single-component systems and cannot be therefore applied to a-C:H studies.

In the case of a-C:H, the complexity of processes governing the final film properties is enormous. The crucial film quantities such as the density, residual stresses and the sp^3 content depend sensitively on the energy and the type of the depositing molecules, the hydrogen concentration in the film, and the temperature. In this ABOP study we have attempted to simulate the evolution of an a-C:H film during deposition of 50 acetylene molecules. In order to investigate the influence of the deposition energy on the film development, we performed two simulation runs with incident acetylene energies of 25 and 100 eV per carbon atom. Before each impact, an acetylene molecule was placed at a random position above the film surface and randomly oriented. Unlike in the study of Marks et al. [56], who used the diamond crystal as a substrate, we have chosen an amorphous substrate with a low density (about 1.7 g/cm^3) and with almost 100% of sp^2 bonded atoms. In this way we were able to detect already after deposition of only several tens of molecules whether the sp^3 to sp^2 ratio in the film remains unchanged or whether it starts to increase.

The structure of the substrate prior the deposition is shown in Fig. 10(a). Initially, the film substrate contained 1345 atoms with 293 hydrogen atoms which corresponds to 21.7% hydrogen concentration. The color coding in Fig. 10 shows the sp^1 bonded atoms in cyan, the sp^2 bonded atoms in yellow, the sp^3 bonded atoms in red, and hydrogens in dark blue. The thickness of the substrate was about 30.0 Å with lateral dimensions of the block of 21.16 Å.

Periodic boundary conditions were applied in directions parallel to the film surface. The impact of the molecule leads to substantial heating of the film. In the case of 25 eV energies the temperature in our sample increased upon deposition to about 600 K, while for 100 eV it exceeded 1500 K. To remove the excess energy before subsequent deposition the bottom part of the film with the thickness of 10 Å acted as a thermostat and was kept at 10 K throughout the whole simulation. In this way the heat can diffuse out of the system and the setup leads to a rather natural cooling of the film without a need to apply velocity rescaling algorithms for all particles. After each deposition the system was let to evolve for 6 ps which was found to be a sufficient time for a spontaneously cooling of the substrate below room temperature in both simulations.

Even though the film growth after only 50 deposited molecules is far from a steady-state, our calculations show both common features and clear differences between the final configurations of both simulation runs. In both cases we observed a gradual increase of the sp^3 content in the films during depositions. The initial sp^3 concentration of 2.9% in the substrate increased to 6.9% and 9.1% in the 25 eV and 100 eV simulations, respectively. The morphology of the final films from the two runs is however markedly different. Fig. 10(b) shows the final configuration of the 25 eV simulation. It is evident that the increase of sp^3 content is localized only in the surface region with the thickness of few Å. The remaining film differs only slightly from the initial substrate. Such behavior is easy to explain. The maximum penetration depth for acetylene molecules with kinetic energies of 25 eV per carbon is about 8 Å in our substrate and the majority of deposited atoms are located 4–6 Å below the film surface. The incoming acetylene molecules have therefore sufficient energy to transform directly only few Å of the film. In contrast, the sp^3 bonded atoms in the final structure from the 100 eV simulation, shown in Fig. 10(c), are distributed uniformly throughout the whole film. The carbon atoms with energies of 100 eV can penetrate up to 20 Å inside the film and generate thus changes in the whole film volume. Furthermore, the upper region of the film is changed dramatically. There are long carbon chains sticking out of the surface and the surface region contains a significant proportion of sp^1 bonded atoms. The energetic impacts of acetylene molecules with 100 eV per carbon atom cause also a formation of local craters and lead to a high number of sputtered atoms. While in both simulations about two thirds of deposited atoms remain in the film, almost 100 atoms were sputtered from the original substrate in the 100 eV simulation. This is five times more than in the 25 eV simulation.

Our present simulations have provided only a limited insight into the mechanisms of a-C:H film growth, and there is a clear need for a continuation and a more detailed analysis. It appears that the ABOP in its current form is able to describe the linear dependence of the sp^3 content on the a-C:H density as well as the influence of the energy of the deposited molecules on the structure of

amorphous network in the growing film which is one of the key experimental results. However, since the variability of a-C:H films is so diverse, a lot more simulations is needed for the final verdict to be made. Finally, it should be mentioned that even though the simulations lasted in real time only 300 ps, the number of time steps exceeded $5 \cdot 10^5$. These calculations thus prove that ABOPs are not only an accurate but also an efficient scheme.

6 Conclusions

In this paper we have presented the latest member of David Pettifor's family of bond order potentials – the ABOP. Our studies of the hydrocarbon system demonstrate that ABOP is able to describe bonding in both solid-state and molecular systems and reproduces to a great extent the TB results. Based on the work of David Pettifor we have extended the σ bond order expression so that it includes explicitly the dependence on the sp splitting of atomic on-site energies which cannot be neglected in the case of carbon. It has been shown that this extension is crucial for the correct description of σ bond order scaling. Additionally, this modification cures the overcoordination in amorphous structures and leads to a correct description of liquid behavior in a close agreement with OTB results.

The accuracy and predictive power of ABOP is currently bound by the limitations of the OTB model and its parameterization. In order to shift from qualitative to quantitative predictions, the original hydrocarbon OTB parameterization has to be reconsidered. From the more fundamental point of view further steps should also head for improvements and extensions of the OTB model itself. The fundamental two-center σ and π bond integrals in two-center OTB schemes are assumed to be simple continuous functions of interatomic distance. In reality, however, these quantities are strongly dependent on the environment [29,57,58]. In a recent study, Mathioudakis et al. [59] have employed the environmentally-dependent OTB model for simulations of amorphous carbon with similar predictive power as NOTB and DFT methods. A rigorous connection between the NOTB and environmentally-dependent OTB schemes has been found by inverting the non-orthogonality matrix using the BOP theory [58]. This derivation leads to explicit analytic expressions for the environmental dependence of the two-center bond integrals within the OTB representation. An extension of the ABOP scheme to include the environmentally-dependent bond integrals would further improve its transferability without sacrificing the models' transparency. Such a robust scheme would then approach the accuracy of NOTB methods at a fraction of their computational costs.

In our simulations, ABOP is currently (without any dedicated optimization

of computer codes) about an order of magnitude slower than the Brenner potential. Apart from the film growth studies we have performed simulations of C_{60} impact onto diamond with more than 50 000 atoms on a modern desktop computer. With ever increasing computer power and employment of parallel computers the performance of ABOPs therefore will not pose a serious problem.

We believe that the future of ABOPs is very bright. With a sound theoretical basis, reliable parameterization and improved efficiency the model can be applied to large-scale atomistic simulations of extreme complexity such as film growth, tribological degradation and polymer physics.

7 Ackowledgments

Financial support for this work was provided by the Fraunhofer Society through the MAVO project "MMM-Tools", and by the Ministry of Economy of the State of Baden-Württemberg through the project "FunkOpti". We would like to thank David Pettifor and Ralf Drautz for valuable comments.

References

[1] N. Dubrovinskaia, L. Dubrovinsky, W. Crichton, F. Langenhorst, A. Richter, Aggregated diamond nanorods, the densest and least compressible form of carbon, Appl. Phys. Lett. 87 (2005) 083106.

[2] M. Dienwiebel, G. S. Verhoeven, N. Pradeep, J. W. M. Frenken, J. A. Heimberg, H. W. Zandbergen, Superlubricity of graphite, Phys. Rev. Lett. 92 (2004) 126101.

[3] M. Moseler, H. Riedel, P. Gumbsch, J. Stäring, B. Mehlig, Understanding the phase transformation from fullerite to amorphous carbon at the microsopic level, Phys. Rev. Lett. 94 (2005) 165503.

[4] M. Zhang, S. L. Fang, A. A. Zakhidov, S. B. Lee, A. E. Aliev, C. D. Williams, K. R. Atkinson, R. H. Baughman, Strong, transparent, multifunctional, carbon nanotube sheets, Science 309 (2005) 1215–9.

[5] M. Moseler, P. Gumbsch, C. Casiraghi, A. C. Ferrari, J. Robertson, The ultrasmoothness of diamond-like carbon surfaces, Science 309 (2005) 1545–8.

[6] P. Hohenberg, W. Kohn, Inhomogeneous electron gas, Phys. Rev. 136 (1964) B864–71.

[7] W. Kohn, L. J. Sham, Self-consistent equations including exchange and correlation effects, Phys. Rev. 140 (1965) A1133–8.

[8] M. S. Tang, C. Z. Wang, C. T. Chan, K. M. Ho, Environment-dependent tight-binding potential model, Phys. Rev. B 53 (1996) 979–82.

[9] C. Goringe, D. Bowler, E. Hernandez, Tight-binding modelling of materials, Rep. Prog. Phys. 60 (1997) 1447–1512.

[10] T. Frauenheim, G. Seifert, M. Elstner, T. Niehaus, C. Köhler, M. Amkreutz, M. Sternberg, Z. Hajnal, A. D. Carlo, S. Suhai, Atomistic simulations of complex materials: ground-state and excited-state properties, J. Phys.: Condens. Matter 14 (2002) 3015–47.

[11] G. C. Abell, Empirical chemical pseudopotential theory of molecular and metallic bonding, Phys. Rev. B 31 (1985) 6184–96.

[12] J. Tersoff, New empirical approach for the structure and energy of covalent systems, Phys. Rev. B 37 (1988) 6991–7000.

[13] D. W. Brenner, Empirical potential for hydrocarbons for use in simulating the chemical vapour deposition of diamond films, Phys. Rev. B 42 (1990) 9458–71.

[14] D. G. Pettifor, New many-body potentials for the bond order, Phys. Rev. Lett. 63 (1989) 2480–3.

[15] D. G. Pettifor, M. Aoki, Angularly dependent many-body potentials within tight-binding Hückel theory, in: J. L. Moran-Lopez, F. Mejia-Lira, J. M. Sanchez (Eds.), Structural and Phase Stability of Alloys, Plenum Press, New York, 1992, pp. 119–32.

[16] P. Alinaghian, P. Gumbsch, A. J. Skinner, D. G. Pettifor, Bond order potentials - a study of s-valent and sp-valent systems, J. Phys.: Condens. Matter 5 (1993) 5795–810.

[17] D. G. Pettifor, I. I. Oleinik, Analytic bond-order potentials beyond Tersoff-Brenner. I. Theory, Phys. Rev. B 59 (1999) 8487–99.

[18] D. G. Pettifor, I. I. Oleinik, Bounded analytic bond-order potentials for σ and π bonds, Phys. Rev. Lett. 84 (2000) 4124–7.

[19] D. G. Pettifor, I. I. Oleinik, Analytic bond-order potential for open and close-packed phases, Phys. Rev. B 65 (2002) 172103.

[20] J. Robertson, Diamond-like amorphous carbon, Mat. Sci. Eng. R 37 (2002) 129–281.

[21] H. U. Jäger, K. Albe, Molecular-dynamics simulations of steady-state growth of ion-deposited tetrahedral amorphous carbon films, J. Appl. Phys. 88 (2000) 1129–35.

[22] N. A. Marks, N. C. Cooper, D. R. McKenzie, D. G. McCulloch, P. Bath, S. P. Russo, Comparison of density-functional, tight-binding, and empirical methods for the simulation of amorphous carbon, Phys. Rev. B 65 (2002) 075411.

[23] D. G. Pettifor, M. W. Finnis, D. Nguyen-Manh, D. A. Murdick, X. W. Zhou, H. N. G. Wadley, Analytic bond-order potentials for multicomponenet systems, Mat. Sci. Eng. A 365 (2004) 2–13.

[24] W. A. Harrison, Electronic Structure and Properties of Solids, Freeman, San Francisco, 1980.

[25] A. P. Sutton, M. W. Finnis, D. G. Pettifor, Y. Ohta, The tight-binding bond model, J. Phys. C: Solid State 21 (1988) 35–66.

[26] W. M. C. Foulkes, R. Haydock, Tight-binding and pair potential, Phys. Rev. B 39 (1989) 12520–36.

[27] M. W. Finnis, Interatomic forces in condensed matter, Oxford University Press, 2003.

[28] D. Nguyen-Manh, D. G. Pettifor, S. Znam, V. Vitek, Negative cauchy pressure within the tight-binding approximation, in: P. E. A. Turchi, A. Gonis, L. Colombo (Eds.), Tight-Binding Approach to Computational Materials Science, Vol. 491, Materials Research Society, Pittsburgh, 1998, pp. 353–8.

[29] M. Mrovec, D. Nguyen-Manh, D. G. Pettifor, V. Vitek, Bond-order potential for molybdenum: Application to dislocation behavior, Phys. Rev. B 69 (2004) 094115.

[30] J. C. Slater, G. F. Koster, Simplified LCAO method for the periodic potential problem, Phys. Rev. 94 (1954) 1498–524.

[31] R. Haydock, Recursion method, in: H. Ehrenreich, D. Turnbull (Eds.), Solid State Physics, Vol. 35, New York, Academic Press, 1980, pp. 216–94.

[32] C. Lanczos, An iteration method for the solution of the eigenvalue problem of linear differential and integral operators, J. Res. Natl. Bur. Stand. 45 (1950) 255–82.

[33] F. Cyrot-Lackmann, Sur le calcul de la cohesion et de la tension superficielle des metaux de transition par une methode de liaisons fortes, J. Phys. Chem. Solids 29 (1968) 1235–43.

[34] F. Ducastelle, F. Cyrot-Lackmann, Moments developments and their application to the electronic charge distribution of d-bands, J. Phys. Chem. Solids 31 (1970) 1295–306.

[35] D. G. Pettifor, M. Aoki, Bonding and structure of intermetallics: a new bond order potential, Philos. Tr. R. Soc. S-A 334 (1991) 439–49.

[36] M. Aoki, Rapidly convergent bond order expansion for atomistic simulations, Phys. Rev. Lett. 71 (1993) 3842–5.

[37] D. G. Pettifor, From exact to approximate theory: The tight binding bond model and many body potentials, in: R. M. Nieminen, J. Puska, M. Manninen (Eds.), Many Atom Interactions in Solids, Vol. 48 of Springer Proceedings in Physics, Springer, Berlin, 1990, pp. 64–84.

[38] P. Alinaghian, S. Nishitani, D. Pettifor, Shear constants using angularly dependent bond order potentials, Phil. Mag. B 69 (1994) 889–900.

[39] R. Drautz, D. A. Murdick, D. Nguyen-Manh, X. W. Zhou, H. N. G. Wadley, D. G. Pettifor, Analytic bond-order potential for predicting structural trends across the sp-valent elements, Phys. Rev. B 72 (2005) 144105.

[40] I. I. Oleinik, D. G. Pettifor, Analytic bond-order potentials beyond Tersoff-Brenner. II. Application to the hydrocarbons, Phys. Rev. B 59 (1999) 8500–7.

[41] C. H. Xu, C. Z. Wang, C. T. Chan, K. M. Ho, A transferable tight-binding potential for carbon, J. Phys.: Condens. Matter 4 (1992) 6047–54.

[42] B. N. Davidson, W. E. Pickett, Tight-binding study of hydrogen on the C(111), C(100), and C(110) diamond surfaces, Phys. Rev. B 49 (1994) 11253–67.

[43] A. P. Horsfield, P. D. Godwin, D. G. Pettifor, A. P. Sutton, Computational materials synthesis. I. A tight-binding scheme for hydrocarbons, Phys. Rev. B 54 (1996) 15773–75.

[44] N. A. Marks, Generalizing the environment-dependent interaction potential for carbon, Phys. Rev. B 63 (2000) 035401.

[45] A. C. T. van Duin, S. Dasgupta, F. Lorant, W. A. Goddard III, ReaxFF: a reactive force field for hydrocarbons, J. Phys. Chem. A 105 (2001) 9396–409.

[46] N. A. Marks, D. R. McKenzie, B. A. Pailthorpe, M. Bernasconi, M. Parinello, *Ab initio* simulations of tetrahedral amorphous carbon, Phys. Rev. B 54 (1996) 9703–14.

[47] T. Frauenheim, P. Blaudeck, U. Stephan, G. Jungnickel, Atomic structure and physical properties of amorphous carbon and its hydrogenated analogs, Phys. Rev. B 48 (1993) 4823–34.

[48] G. Jungnickel, T. Frauenheim, D. Porezag, P. Blaudeck, U. Stephan, R. J. Newport, Structural properties of amorphous hydrogenated carbon. IV. A molecular-dynamics investigation and comparison to experiments, Phys. Rev. B 50 (1994) 6709–16.

[49] P. D. Godwin, A. P. Horsfield, A. M. Stoneham, S. J. Bull, I. J. Ford, A. H. Harker, D. G. Pettifor, A. P. Sutton, Computational materials synthesis. III. Synthesis of hydrogenated amorphous carbon from molecular precursors, Phys. Rev. B 54 (1996) 15785–94.

[50] M. M. M. Bilek, D. R. McKenzie, D. G. McCulloch, C. M. Goringe, *Ab initio* simulation of structure in amorphous hydrogenated carbon, Phys. Rev. B 62 (2000) 3071–7.

[51] S. J. Stuart, A. B. Tutein, J. A. Harrison, A reactive potential for hydrocarbons with intermolecular interactions, J. Chem. Phys. 112 (2000) 6472–86.

[52] D. W. Brenner, O. A. Shenderova, J. A. Harrison, S. J. Stuart, B. Ni, S. B. Sinnott, A second-generation reactive empirical bond order (REBO) potential energy expression for hydrocarbons, J. Phys.: Condens. Matter 14 (2002) 783–802.

[53] A. C. Ferrari, et al., Density, sp^3 fraction, and cross-sectional structure of amorphous carbon films determined by x-ray reflectivity and electron energy-loss spectroscopy, Phys. Rev. B 62 (2000) 11089–103.

[54] J. K. Walters, P. J. R. Honeybone, D. W. Huxley, R. J. Newport, W. S. Howells, Structural properties of amorphous hydrogenated carbon. I. A high-resolution neutron-diffraction study, Phys. Rev. B 50 (1994) 831–8.

[55] K. Nordlund, J. Keinonen, T. Mattila, Formation of ion induced small-scale defects on graphite surfaces, Phys. Rev. Lett. 77 (1996) 699–702.

[56] N. A. Marks, J. M. Bell, G. K. Pearce, D. R. McKenzie, M. M. M. Bilek, Atomistic simulation of energy and temperature effects in the deposition and implantation of amorphous carbon thin films, Diam. Relat. Mater. 12 (2003) 2003–10.

[57] H. Haas, C. Z. Wang, M. Fähnle, C. Elässser, K. Ho, Environment-dependent tight-binding model for molybdenum, Phys. Rev. B 57 (1998) 1461–70.

[58] D. Nguyen-Manh, D. Pettifor, V. Vitek, Analytic environment-dependent tight-binding bond integrals: Application to $MoSi_2$, Phys. Rev. Lett. 85 (2000) 4136–9.

[59] C. Mathioudakis, G. Kopidakis, P. C. Kelires, C. Z. Wang, K. M. Ho, Physical trends in amorphous carbon: A tight-binding molecular-dynamics study, Phys. Rev. B 70 (2004) 125202.